Long-Range Multibody Interactions and Three-Body Antiblockade in a Trapped Rydberg Ion Chain

Filippo M. Gambetta,[1,2] Chi Zhang,[3] Markus Hennrich,[3] Igor Lesanovsky,[1,2,4] and Weibin Li[1,2]
[1]School of Physics and Astronomy, University of Nottingham, Nottingham, NG7 2RD, United Kingdom
[2]Centre for the Mathematics and Theoretical Physics of Quantum Non-equilibrium Systems, University of Nottingham, Nottingham NG7 2RD, United Kingdom
[3]Department of Physics, Stockholm University, 10691 Stockholm, Sweden
[4]Institut für Theoretische Physik, University of Tübingen, 72076 Tübingen, Germany

(Received 18 May 2020; accepted 27 August 2020; published 22 September 2020)

Trapped Rydberg ions represent a flexible platform for quantum simulation and information processing that combines a high degree of control over electronic and vibrational degrees of freedom. The possibility to individually excite ions to high-lying Rydberg levels provides a system where strong interactions between pairs of excited ions can be engineered and tuned via external laser fields. We show that the coupling between Rydberg pair interactions and collective motional modes gives rise to effective long-range and multibody interactions consisting of two, three, and four-body terms. Their shape, strength, and range can be controlled via the ion trap parameters and strongly depends on both the equilibrium configuration and vibrational modes of the ion crystal. By focusing on an experimentally feasible quasi one-dimensional setup of $^{88}Sr^{+}$ Rydberg ions, we demonstrate that multibody interactions are enhanced by the emergence of soft modes associated with, e.g., a structural phase transition. This has a striking impact on many-body electronic states and results—for example—in a three-body antiblockade effect that can be employed as a sensitive probe to detect structural phase transitions in Rydberg ion chains. Our study unveils the possibilities offered by trapped Rydberg ions for studying exotic phases of matter and quantum dynamics driven by enhanced multibody interactions.

DOI: 10.1103/PhysRevLett.125.133602

Introduction.—The coupling between internal atomic states and collective vibrational modes is the hallmark of trapped ion setups. The possibility to engineer tunable phonon-mediated two-body interactions, combined with single-ion control and high fidelity state preparation, makes them a powerful platform for quantum simulation and information processing [1–14]. A further enhancement of this setup can be achieved in trapped Rydberg ions, where each ion can be individually excited to a high-lying Rydberg level [15–23]. The strong dipole-dipole interactions and the interplay between electronic and vibrational degrees of freedom characterizing this system can be exploited to simulate equilibrium and nonequilibrium quantum many-body spin models [24–26], to devise nonclassical motional states [27], and for quantum information processing beyond the scalability limitations of conventional ion settings [28–30].

In this Letter, we demonstrate that the unique intertwining between intrinsically collective vibrational motion and dipole-dipole interactions characterizing trapped Rydberg ions provides a mechanism to engineer long-range and multibody interactions in state-of-the-art setups. With respect to their neutral counterparts, Rydberg ions offer important experimental advantages. They can be conveniently trapped via state-independent electric potentials and do not require magic trapping conditions [31–33], while the control over both electronic and vibrational degrees of freedom allows the manipulation of their state with an unprecedented degree of fidelity. We investigate the emergence of multibody interactions by focusing on a chain of $^{88}Sr^{+}$ Rydberg ions confined by harmonic potentials [see Fig. 1(a)], which has been recently experimentally realized [30]. We demonstrate that their strength is significantly enhanced in the presence of soft vibrational modes. These occur, e.g., at the linear-to-zigzag transition in a chain of a few ions [34–40] and in long linear chains. Here, interactions induced by spin-phonon coupling give rise to nontrivial many-body phenomena, such as a three-body antiblockade effect. The novel capabilities we unveil in our work show that trapped Rydberg ions are a powerful platform for quantum simulation, allowing for the study of exotic kinetically constrained dynamics [41,42], long-lived quantum information storage [43], and correlated quantum states of matter [44–51].

Spin-phonon coupling induced multibody interactions.—We consider a quasi one-dimensional chain of N two-level Rydberg ions confined by a harmonic potential, as sketched in Fig. 1(a). The two levels (with $|\downarrow\rangle$ and $|\uparrow\rangle$ denoting the ground and Rydberg states, respectively) are coupled by a

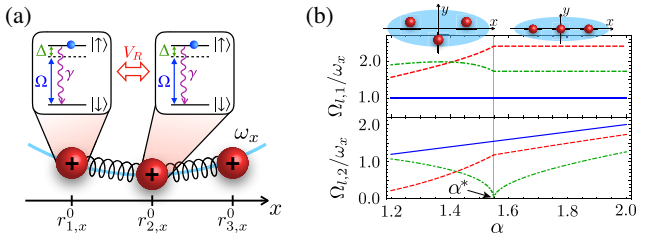

FIG. 1. Setup and phonon eigenfrequencies of a three-ion crystal. (a) Ions are modeled as two-level systems whose ground state $|\downarrow\rangle$ is coupled to a Rydberg state $|\uparrow\rangle$ by a laser with Rabi frequency Ω and detuning Δ. The state $|\uparrow\rangle$ spontaneously decays to $|\downarrow\rangle$ with rate γ. The equilibrium positions $\boldsymbol{r}_n^0$ are determined by the interplay between Coulomb repulsion and harmonic confinement. Ions m and n interact through the interaction potential $V_R(\boldsymbol{r}_n, \boldsymbol{r}_m)$ when both are excited to Rydberg states. (b) Eigenfrequencies $\Omega_{l,\lambda}$ as a function of the trap aspect ratio $\alpha = \omega_y/\omega_x$ ($l = 1$ blue solid, $l = 2$ red dashed, $l = 3$ green dash-dotted). For $\alpha > \alpha^*$, the upper plot ($\Omega_{l,1}/\omega_x$) corresponds to longitudinal phonon modes, while the lower one ($\Omega_{l,2}/\omega_x$) displays the transverse ones. The gray line highlights the structural phase transition at $\alpha^* = \sqrt{12/5}$. The configurations of a three-ion chain are sketched on the top. The shaded blue areas represent the trapping region in the $x - y$ plane.

laser field with Rabi frequency Ω and detuning Δ. The overall Hamiltonian is

$$H = H_{\text{ions}} + H_L + H_{\text{int}}, \tag{1}$$

with $H_{\text{ions}} = \sum_{l,\lambda} \hbar\Omega_{l,\lambda}(a^\dagger_{l,\lambda} a_{l,\lambda} + 1/2)$ describing the vibrational dynamics of an ion crystal confined in a three-dimensional harmonic potential $v_\mu(r_{n,\mu}) = M\omega_\mu^2 r_{n,\mu}^2/2$. Here, $\boldsymbol{r}_n$ is the nth ion position, M its mass, and ω_μ the trapping frequency along direction $\mu = \{x, y, z\}$ [40,52,53]. Bosonic operators $a^{(\dagger)}_{l,\lambda}$ are associated with the phonon mode (l, λ) with eigenfrequency $\Omega_{l,\lambda}$, where λ labels the phonon branches [54]. We assume $\omega_{x,y} \ll \omega_z$, so that the motion of the ions is confined to the $x - y$ plane. In Eq. (1), $H_L = \sum_{n=1}^N [\Omega\sigma_n^x + \Delta n_n]$ describes the laser excitation of ions to the Rydberg state. Here, $n_n = (1 + \sigma_n^z)/2$ and σ_n^μ are the Rydberg number operator and Pauli matrices acting on the nth ion, respectively. The electrostatic dipole-dipole interaction between pairs of Rydberg excited ions is modeled by $H_{\text{int}} = \sum'_{m,n} V_R(\boldsymbol{r}_m, \boldsymbol{r}_n) n_m n_n$, where $V_R(\boldsymbol{r}_m, \boldsymbol{r}_n) = V_R(|\boldsymbol{r}_m - \boldsymbol{r}_n|)$ and the prime denotes $m \neq n$. Under typical experimental conditions, the displacements of ions from their equilibrium positions $\boldsymbol{r}_n^0$ are much smaller than inter-ion distances. Hence, we expand $V_R(\boldsymbol{r}_m, \boldsymbol{r}_n)$ to first order around $\boldsymbol{r}_n^0$ [33,54]. By substituting the expansion into Eq. (1) and performing a polaron transformation to approximately decouple electronic and vibrational degrees of freedom [5,6,33,54], Eq. (1) becomes

$$H' \simeq H_{\text{ions}} + H_{\text{spin}} + H_{\text{res}}. \tag{2}$$

The spin Hamiltonian $H_{\text{spin}} = H_L + H^0_{\text{int}} + H^{\text{eff}}_{\text{int}}$ contains, in addition to the bare dipole-dipole interaction term $H^0_{\text{int}} = \sum'_{m,n} V_R(\boldsymbol{r}_m^0, \boldsymbol{r}_n^0) n_m n_n$, also an *effective* Rydberg interaction contribution

$$H^{\text{eff}}_{\text{int}} = -\sum\nolimits_{m,n}{}' \sum\nolimits_{i,j}{}' \tilde{V}_{mnij} n_m n_n n_i n_j \tag{3}$$

generated as a consequence of the polaron transformation. $H^{\text{eff}}_{\text{int}}$ consists of long-range and multibody interactions coupling two, three, and four spins. Their strength is encoded in the effective interaction (EI) coefficients

$$\tilde{V}_{mnij} = \frac{2}{M} G_{mn} G_{ij} \sum_{\mu,\nu} F^{\mu\nu}_{mi} \bar{R}^0_{mn;\mu} \bar{R}^0_{ij;\nu}, \tag{4}$$

where we defined $\nabla_{r_{m,\mu}} V_R(\boldsymbol{r}_m, \boldsymbol{r}_n^0)|_{\boldsymbol{r}_m^0} \equiv G_{mn}\bar{\boldsymbol{R}}^0_{mn}$, with coefficients G_{mn} describing the magnitude of the gradient of the Rydberg potential and factors $\bar{\boldsymbol{R}}^0_{mn} = (\boldsymbol{r}_m^0 - \boldsymbol{r}_n^0)/|\boldsymbol{r}_m^0 - \boldsymbol{r}_n^0|$ encoding the geometry of the system. EIs explicitly depend on the trapping regime via the coupling parameters $F^{\mu\nu}_{mi} = \sum_{l,\lambda} \Omega^{-2}_{l,\lambda} \mathcal{M}^{\mu\lambda}_{ml} \mathcal{M}^{\nu\lambda}_{il}$, where the normal mode matrices $\mathcal{M}^{\mu\lambda}_{ml}$ relate local ion displacements to chain normal modes [54]. Hence, the coefficients $\tilde{V}_{mnij}$ can be controlled by both the Rydberg interaction potential, through its gradient coefficients G_{mn}, and the vibrational structure of the chain. In Eq. (2), H_{res} contains a residual spin-phonon interaction [5,6,54]. In the strong interaction regime, which will be the focus of subsequent sections, its contribution to the spin dynamics is negligible when $\Omega \ll \Omega^* \sim \min(\Omega^{-1/2}_{l,\lambda})$ [54]. In this case, the electronic and vibrational degrees of freedom decouple.

Three-ion chain.—We first investigate the onset of EIs in a three-ion setting, in which $H^{\text{eff}}_{\text{int}}$ reads

$$H^{\text{eff}}_{\text{int}} = -C^{2\text{b}}_{\text{NN}}(n_1 n_2 + n_2 n_3) - C^{2\text{b}}_{\text{NNN}} n_1 n_3 - C^{3\text{b}} n_1 n_2 n_3.$$

The coefficients $C^{2\text{b}}_{\text{NN}}$ and $C^{2\text{b}}_{\text{NNN}}$ parameterize two-body EIs between nearest neighbors (NNs) and next-to-nearest neighbors (NNNs), respectively, while $C^{3\text{b}}$ describes the three-body contribution. Their behavior in the various trapping regimes can be inferred from Eq. (4). A three-ion chain features a second-order phase transition to a zigzag configuration at the critical value $\alpha^* = \sqrt{12/5}$ of the trap aspect ratio $\alpha = \omega_y/\omega_x$ [40,54]. The transition is signaled by the emergence of a *soft mode* with eigenfrequency $\Omega_{3,2} \to 0$ [see Fig. 1(b)], which, depending on the configuration of the ions, may strongly affect the EIs. In the linear regime ($\alpha > \alpha^*$), the longitudinal and transverse modes of the chain are not coupled and the normal mode matrices $\mathcal{M}^{\mu\lambda}_{ml}$ vanish when $\mu \neq \lambda$ [54]. In this case, the soft

mode is purely transverse and, since $\bar{R}_{mn;y} \propto r^0_{m,y} - r^0_{m,y} = 0$, it does not contribute to $\tilde{V}_{mnij}$. This traces back to the fact that transverse displacements hardly affect inter-ion distances and only generate higher-order terms in the expansion of $V_R(\boldsymbol{r}_m, \boldsymbol{r}_n)$: In a linear chain only longitudinal modes contribute to $\tilde{V}_{mnij}$ via the coupling parameter F^{xx}_{mi}. As show in Fig. 1(b), the latter are constant as a function of α and only depend on ω_x as $F^{xx}_{mi} \propto \Omega_{l,1} \sim \omega_x^{-2}$. We note that, for $\alpha > \alpha^*$, ω_x uniquely determines the distances between ions, which scale as $\omega_x^{-2/3}$ [54]. Since for dipole-dipole interaction potentials larger distances result in smaller gradients, in a three-ion chain it is not possible to arbitrarily "soften" the longitudinal modes, and thus the magnitude of the EIs that can be achieved is strongly limited. In the zigzag configuration ($\alpha < \alpha^*$), on the contrary, all normal modes possess both longitudinal and transverse components, i.e., $\mathcal{M}^{\mu\lambda}_{ml} \neq 0$, $\forall\, \mu, \lambda$ [54]. The collective and intertwined nature of phonon modes results in nonvanishing coupling parameters $F^{\mu\nu}_{mi}$, $\forall\, \mu, \nu$. Moreover, $\bar{R}_{mn;y} \neq 0$ and hence all the couplings $F^{\mu\nu}_{mi}$ contribute to Eq. (4). Crucially, due to the presence of the soft mode (3,2), for $\alpha \to (\alpha^*)^-$ one finds $F^{\mu\nu}_{mi} \sim \Omega^{-2}_{3,2}$, $\forall\, \mu, \nu$. We therefore expect an increase of the EI strength close to the critical point.

Looking at Eq. (4), one notices that large Rydberg potential gradients G_{mn} are essential to maximize the effects of EIs. Unfortunately, in trapped Rydberg ions, van der Waals interactions are generally weaker than their neutral counterparts and do not give access to large gradients. To overcome this issue, we exploit the interplay between dipole-dipole interactions of microwave (MW) dressed states [19,28] and MW-tuned Förster resonance in a setup of $^{88}Sr^+$ trapped Rydberg ions [21,22,30]. This allows us to obtain the ion-ion interaction potential shown in Fig. 2(a) [54]. The corresponding EI coefficients are shown in Fig. 2(b) as a function of the trap aspect ratio α. For

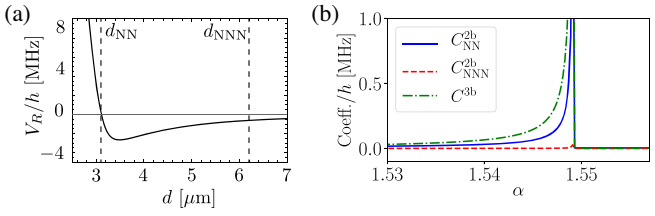

FIG. 2. Effective multibody interaction in a three-ion chain. (a) Two-ion MW dressed potential $V_R(d)$ as a function of the ion separation d [54]. Dashed gray lines denote the distance between NNs, $d_{\rm NN} = 3.1$ μm, and NNNs, $d_{\rm NNN} = 2d_{\rm NN}$, in a linear chain with $\omega_x = 2\pi \times 1.3$ MHz. Here, $V_{\rm NN}/h = 0.25$ MHz and $V_{\rm NNN}/h = -0.6$ MHz, with corresponding gradients $G_{\rm NN}/h = 23.6$ MHz/μm and $G_{\rm NNN}/h = 0.3$ MHz/μm. (b) EI coefficients associated with the potential in panel (a) as a function of the trap aspect ratio α. The emergence of a soft mode at the linear-to-zigzag transition leads to a significant enhancement of the EIs.

$\alpha > \alpha^*$ their values are fixed and small, as expected from the discussion above. On the other hand, for $\alpha \to (\alpha^*)^-$, the two-dimensional configuration of the chain, the mixing between longitudinal and transversal modes, and the emergence of a soft mode result in a significant enhancement of the EI strength. The sign of interaction coefficients is determined by the gradient of the Rydberg potential at NNs and NNNs $G_{\rm NN}$ and $G_{\rm NNN}$ respectively. The potential chosen in Fig. 2(a) gives $G_{\rm NN} < 0$ and $G_{\rm NNN} > 0$. Close to the linear-to-zigzag transition, this results in $C^{2b}_{\rm NN}, C^{2b}_{\rm NNN}, C^{3b} > 0$ [see Fig. 2(b)], corresponding to attractive EIs.

We now investigate an interaction induced three-body Rydberg antiblockade regime, a generalization of the well-studied facilitation mechanism in the presence of two-body Rydberg interactions [56–60]. By denoting with $V_{\rm NN}$ and $V_{\rm NNN}$ the bare Rydberg interactions between NNs and NNNs contained in $H^0_{\rm int}$, respectively, this regime is achieved when [see the level structure in Fig. 3(a)]

$$3\Delta + 2(V_{\rm NN} - C^{2b}_{\rm NN}) + (V_{\rm NNN} - C^{2b}_{\rm NNN}) - C^{3b} = 0. \quad (5)$$

If ions are prepared in state $|\downarrow\downarrow\downarrow\rangle$ at time $t = 0$, an enhancement in the projector on state $|\uparrow\uparrow\uparrow\rangle$ at subsequent times $P_{\uparrow\uparrow\uparrow}(t)$ is expected for values of Δ satisfying Eq. (5). The behavior of the time-integrated expectation value of

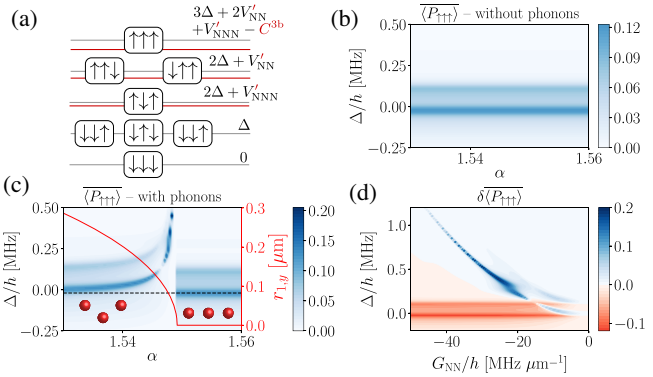

FIG. 3. Three-body spectroscopy. (a) Electronic levels of a three-ion chain. Here, $V'_{\rm NN} = V_{\rm NN} - C^{2b}_{\rm NN}$ and $V'_{\rm NNN} = V_{\rm NNN} - C^{2b}_{\rm NNN}$. Red (gray) lines correspond to energy levels in the presence (absence) of EIs in the regime of Fig. 2(b). (b), (c) Time-integrated expectation value of $P_{\uparrow\uparrow\uparrow}$ as a function of trap aspect ratio α and detuning Δ/h for a system of $N = 3$ ions without (b) and with (c) EIs. The initial state is $|\downarrow\downarrow\downarrow\rangle$ and $\Omega/h = 0.1$ MHz. Other parameters are as in Fig. 2. Time averages are evaluated over a 50 μs window, and we included the finite Rydberg lifetime $\tau = \gamma^{-1} = 30$ μs [see Fig. 1(a)]. In (c), the red solid curve shows the transverse displacement $r_{1,y} = r_{3,y}$ as a function of α [54], while the black dashed line highlights the position of the maximum of $\overline{\langle P_{\uparrow\uparrow\uparrow}\rangle}$ from panel (b). (d) Difference between the time-averaged expectation values of $P_{\uparrow\uparrow\uparrow}$ with and without EIs as a function of $G_{\rm NN}/h$ and Δ/h for $\alpha = 1.548$. Here, $G_{\rm NNN} = 0.01 G_{\rm NNN}$. Other parameters are as in (b),(c).

$P_{\uparrow\uparrow\uparrow}(t)$, denoted by $\langle P_{\uparrow\uparrow\uparrow}\rangle$, is shown in Fig. 3(b),(c). Panel (b) shows the case with bare Rydberg interactions only (i.e., with $C^{2b}_{NN} = C^{2b}_{NNN} = C^{3b} = 0$), while effects of EIs are displayed in panel (c). For $\alpha \to (\alpha^*)^-$, EIs modify significantly the value of Δ satisfying Eq. (5). This results in a shift of the peak of $\overline{\langle P_{\uparrow\uparrow\uparrow}\rangle}$. As shown in Fig. 3(d), displaying the difference $\delta\overline{\langle P_{\uparrow\uparrow\uparrow}\rangle}$ between the time-integrated expectation values of $P_{\uparrow\uparrow\uparrow}(t)$ with and without the contributions of $H^{\rm eff}_{\rm int}$, the presence of phonon-mediated EIs leads to a clear spectroscopic signature.

The latter provides a sensitive tool to locate the critical point of the linear-to-zigzag transition, allowing for a significant improvement over state-of-the-art methods [38,61,62]. Indeed, the typical resolution of current direct camera images of the ions is ≈ 0.5 μm and, the transition being a second-order one, they can hardly reveal the small ion displacements along the traverse direction for $\alpha \approx \alpha^*$. In contrast, from Fig. 3(c) we see that close to the critical point a traverse displacement of ≈ 0.1 μm corresponds to a shift of ≈ 0.2 MHz in the peak of $\overline{\langle P_{\uparrow\uparrow\uparrow}\rangle}$, which can be easily detected via spectroscopic measurements [63].

Infinite linear chain.—In the previous section, we showed that in a three-ion chain phonon-mediated EIs are strongly amplified by the emergence of a soft mode. We now inspect the behavior of $H^{\rm eff}_{\rm int}$ in longer chains, where system properties explicitly depend on the number of ions, N [36,37,64]. In particular, by increasing N, one can decrease the inter-ion distance in the central region of the chain even in the presence of a weak longitudinal confinement. This can be exploited to engineer soft modes even in the linear configuration and, hence, it allows one to overcome the restrictions on the strength of EIs we discussed for a linear three-ion chain. As we will show, the increased flexibility provided by a denser vibrational spectrum also provides a convenient handle to control the range of the EIs.

To gain insights into the phenomenology of this case, we consider the infinite chain limit $N \to \infty$, which provides a good description of the central region of long yet finite chains [39,65]. In the linear regime [40], the equilibrium positions of the ions are $\boldsymbol{r}^0_n = (nd, 0)$, with d being the fixed inter-ion distance and $n \in \{0, \pm 1, \ldots, \pm\infty\}$. To mimic the effect of a longitudinal confinement, we replace the harmonic trapping potential along the x axis with a periodic one commensurate with the lattice spacing, $v_x(r_{n,x}) = -M\omega_x(d/2\pi)^2 \cos(2\pi r^0_{n,x}/d)$. Expanding the ions' coordinates in Fourier modes and generalizing the steps leading to Eq. (2), we obtain a Hamiltonian H' with the same form as Eq. (2) [54]. Similarly to the three-ion case, in the linear configuration longitudinal and transverse modes are not coupled (i.e., $F^{\mu\nu}_{mi} = 0$ for $\mu \neq \nu$) and $\bar{R}^0_{mn;y} = 0$. Thus, only longitudinal modes contribute to $\tilde{V}_{mnij}$ via $F^{xx}_{mi} \equiv F(s) = (2\pi)^{-1}\int_{-\pi}^{\pi} dk[\Omega_x(k)]^{-2}e^{-iks}$, with $s = m - i$, $-\pi \leq k < \pi$ defining the wave vector of the first Brillouin zone and $\Omega_x(k)$ the eigenfrequency of phonon mode (k, x) [54].

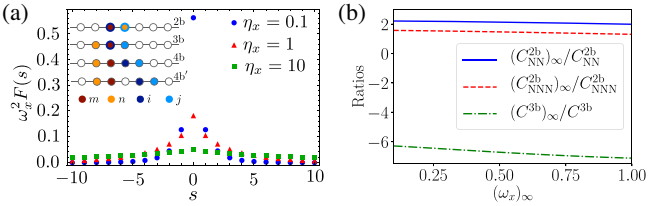

FIG. 4. Effective multibody interactions in an infinite linear chain. (a) Coupling parameters $\omega_x^2 F(s)$ as a function of $s = m - i$ for $\eta_x = 0.1$ (stiff regime), $\eta_x = 1$ (intermediate regime), $\eta_x = 10$ (soft regime). Inset: Examples of possible contributions to $H^{\rm eff}_{\rm int}$. In the stiff limit, the 4b′ term is strongly suppressed with respect to the 4b one. (b) Ratios between the EI coefficients in a linear infinite chain and the corresponding ones for the three-ion case as a function of the infinite chain trapping frequency, $(\omega_x)_\infty$ (units $2\pi \times$ MHz). Distance between NNs is fixed as $d = 3.1$ μm (corresponding to $\omega_x = 2\pi \times 1.3$ MHz for the three-ion chain). Rydberg potential parameters are as in Fig. 2, while $\eta_x > 1$ and $N > 4$ throughout the whole range of $(\omega_x)_\infty$ considered.

The dense vibrational spectrum leads to two different regimes for the ion dynamics that can be controlled via the trap parameter $\eta_x = V_0/(Md^3\omega_x^2)$ [6] and that allows one to substantially modify the behavior of $F(s)$ [see Fig. 4(a)]. For $\eta_x \ll 1$ (stiff limit), ions behave as independent harmonic oscillators, while for $\eta_x \gg 1$ (soft limit) phonon modes describe genuinely collective excitations. In the stiff limit, $F(s)$ is peaked around $s = 0$, implying that dominant contributions to $H^{\rm eff}_{\rm int}$ consist of connected strings of neighboring two-, three-, and four-body terms. On the other hand, for $\eta_x \gtrsim 1$, $F(s)$ has a broader distribution and is nonnegligible also for $|s| > 0$. As a consequence, exotic long-range and multibody interaction terms arise in $H^{\rm eff}_{\rm int}$, as shown in the bottom row of the inset in Fig. 4(a). This broad spectrum of possible interaction patterns, allowed by the collective nature of phonon modes and the precise control over the chain trapping parameters, is in contrast with the case of Rydberg atom tweezer arrays, where only short-range two- and three-body interactions can be engineered [33].

Three-body spectroscopy of a long chain.—The previous discussion allows one to gain an understanding of the three-body spectroscopy of a long yet finite chain, which can be experimentally investigated in trapped Rydberg ion simulators. Indeed, in a long enough chain, long wavelength soft modes, which give the largest contribution to $H^{\rm eff}_{\rm int}$, coincide with good approximation with the ones of the corresponding infinite chain limit [39,65]. Moreover, due to the finite lifetime of Rydberg excitations $\tau = \gamma^{-1}$, with γ the spontaneous decay rate [see Fig. 1(a)], the vibrational spectrum of the chain can be considered as continuous when energy

gaps between phonon modes are smaller than γ. For $^{88}Sr^{+}$ ions (with $\tau \approx 30\ \mu s$) in a trap with $\omega_x = 2\pi \times 0.2$ MHz, the above conditions are both met for chains with $N \gtrsim 20$, which are within the reach of current state-of-the-art setups [30]. The possibility to control inter-ion distances in the central region of a long chain by tuning N allows one to employ a weaker longitudinal confinement, which results in the emergence of soft modes $\Omega_x(k) \sim \omega_x$ near $k \approx 0$. Thus, an enhancement of the EIs can be obtained even in the linear configuration. To quantify this effect, in Fig. 4(b) we plot the ratio between the EI coefficients for an infinite chain and the corresponding ones for the three-ion setup shown in Fig. 2(b). To make the comparison meaningful, we fix the inter-ion distance in the infinite chain as $d = d_{\mathrm{NN}}$, with d_{NN} as in Fig. 2. When the infinite chain trapping frequency $(\omega_x)_\infty$ is varied, d can be kept fixed by adjusting N. In principle, by adding more ions to the chain while keeping $(\omega_x)_\infty$ constant, smaller values of d can be accessed, leading to stronger EIs. Looking at Fig. 4(b), we also note that in an infinite chain $C^{2b}_{\mathrm{NN(N)}}$ and C^{3b} have opposite signs. This fact, due to the different vibrational structure, allows one to investigate the competition between attractive and repulsive EIs. We therefore expect that trapped Rydberg ions will give access to different interaction regimes, paving the way to the study of quantum magnetism and frustration phenomena in the presence of exotic multibody effects.

Conclusions.—We investigated the emergence of long-range multibody interactions in a chain of trapped Rydberg ions induced by the coupling between phonon modes and ion-ion Rydberg interactions. We showed that these interactions are extremely sensitive to the chain equilibrium configuration and vibrational regimes, such as the emergence of soft modes. By employing realistic parameters from a state-of-the-art setup of $^{88}Sr^{+}$ Rydberg ions, we demonstrated that they result in a neat signature of the linear-to-zigzag transition in the spectroscopic signal of the ions' Rydberg state. The intertwining between chain configuration, vibrational structure, and effective interactions illustrated in this Letter provides a versatile mechanism to investigate quantum dynamics in the presence of nontrivial multibody interactions and exotic constraints.

The research leading to these results has received funding from EPSRC Grants No. EP/M014266/1 and No. EP/R04340X/1 (via the QuantERA project "ERyQSenS"), and the Deutsche Forschungsgemeinschaft (DFG) within the SPP 1929 Giant interactions in Rydberg Systems (GiRyd) as well as through the project No. LE 3522/2-1. C. Z. and M. H. acknowledge support from the Swedish Research Council (TRIQS), the QuantERA ERA-NET Cofund in Quantum Technologies (ERyQSenS), and the Knut and Alice Wallenberg Foundation (WACQT). C. Z. acknowledges the hospitality of the University of Nottingham. I. L. acknowledges funding from the "Wissenschaftler Rückkehrprogramm GSO/CZS" of the Carl-Zeiss-Stiftung and the German Scholars Organization e.V., as well as through the Leverhulme Trust (Grant No. RPG-2018-181). W. L. acknowledges funding from the UKIERI-University Grants Commission Thematic Partnership No. IND/CONT/G/16-17/73 and the Royal Society through the International Exchanges Cost Share Grant No. IEC\NSFC\181078.

[1] J. I. Cirac and P. Zoller, Phys. Rev. Lett. **74**, 4091 (1995).
[2] H. Häffner, C. F. Roos, and R. Blatt, Phys. Rep. **469**, 155 (2008).
[3] R. Blatt and D. Wineland, Nature (London) **453**, 1008 (2008).
[4] C. D. Bruzewicz, J. Chiaverini, R. McConnell, and J. M. Sage, Appl. Phys. Rev. **6**, 021314 (2019).
[5] D. Porras and J. I. Cirac, Phys. Rev. Lett. **92**, 207901 (2004).
[6] X.-L. Deng, D. Porras, and J. I. Cirac, Phys. Rev. A **72**, 063407 (2005).
[7] A. Friedenauer, H. Schmitz, J. T. Glueckert, D. Porras, and T. Schaetz, Nat. Phys. **4**, 757 (2008).
[8] K. Kim, M.-S. Chang, R. Islam, S. Korenblit, L.-M. Duan, and C. Monroe, Phys. Rev. Lett. **103**, 120502 (2009).
[9] K. Kim, M. S. Chang, S. Korenblit, R. Islam, E. E. Edwards, J. K. Freericks, G. D. Lin, L. M. Duan, and C. Monroe, Nature (London) **465**, 590 (2010).
[10] K. Kim, S. Korenblit, R. Islam, E. E. Edwards, M.-S. Chang, C. Noh, H. Carmichael, G.-D. Lin, L.-M. Duan, C. C. J. Wang, J. K. Freericks, and C. Monroe, New J. Phys. **13**, 105003 (2011).
[11] R. Islam, E. E. Edwards, K. Kim, S. Korenblit, C. Noh, H. Carmichael, G. D. Lin, L. M. Duan, C. C. J. Wang, J. K. Freericks, and C. Monroe, Nat. Commun. **2**, 377 (2011).
[12] J. W. Britton, B. C. Sawyer, A. C. Keith, C. C. J. Wang, J. K. Freericks, H. Uys, M. J. Biercuk, and J. J. Bollinger, Nature (London) **484**, 489 (2012).
[13] A. Bermudez, J. Almeida, F. Schmidt-Kaler, A. Retzker, and M. B. Plenio, Phys. Rev. Lett. **107**, 207209 (2011).
[14] C. Monroe, W. C. Campbell, L. M. Duan, Z. X. Gong, A. V. Gorshkov, P. Hess, R. Islam, K. Kim, G. Pagano, P. Richerme, C. Senko, and N. Y. Yao, arXiv:1912.07845.
[15] T. F. Gallagher, Rep. Prog. Phys. **51**, 143 (1988).
[16] T. F. Gallagher, *Rydberg Atoms* (Cambridge University Press, New York, 2005).
[17] M. Saffman, T. G. Walker, and K. Mølmer, Rev. Mod. Phys. **82**, 2313 (2010).
[18] R. Löw, H. Weimer, J. Nipper, J. B. Balewski, B. Butscher, H. P. Büchler, and T. Pfau, J. Phys. B **45**, 113001 (2012).
[19] M. Müller, L. Liang, I. Lesanovsky, and P. Zoller, New J. Phys. **10**, 093009 (2008).
[20] F. Schmidt-Kaler, T. Feldker, D. Kolbe, J. Walz, M. Müller, P. Zoller, W. Li, and I. Lesanovsky, New J. Phys. **13**, 075014 (2011).
[21] G. Higgins, W. Li, F. Pokorny, C. Zhang, F. Kress, C. Maier, J. Haag, Q. Bodart, I. Lesanovsky, and M. Hennrich, Phys. Rev. X **7**, 021038 (2017).
[22] G. Higgins, F. Pokorny, C. Zhang, Q. Bodart, and M. Hennrich, Phys. Rev. Lett. **119**, 220501 (2017).

[23] A. Mokhberi, J. Vogel, J. Andrijauskas, P. Bachor, J. Walz, and F. Schmidt-Kaler, J. Phys. B **52**, 214001 (2019).
[24] J. P. Hague and C. MacCormick, New J. Phys. **14**, 033019 (2012).
[25] R. Nath, M. Dalmonte, A. W. Glaetzle, P. Zoller, F. Schmidt-Kaler, and R. Gerritsma, New J. Phys. **17**, 065018 (2015).
[26] F. M. Gambetta, I. Lesanovsky, and W. Li, Phys. Rev. A **100**, 022513 (2019).
[27] W. Li and I. Lesanovsky, Phys. Rev. Lett. **108**, 023003 (2012).
[28] W. Li and I. Lesanovsky, Appl. Phys. B **114**, 37 (2014).
[29] J. Vogel, W. Li, A. Mokhberi, I. Lesanovsky, and F. Schmidt-Kaler, Phys. Rev. Lett. **123**, 153603 (2019).
[30] C. Zhang, F. Pokorny, W. Li, G. Higgins, A. Pöschl, I. Lesanovsky, and M. Hennrich, Nature (London) **580**, 345 (2020).
[31] S. Zhang, F. Robicheaux, and M. Saffman, Phys. Rev. A **84**, 043408 (2011).
[32] D. Barredo, V. Lienhard, P. Scholl, S. de Léséleuc, T. Boulier, A. Browaeys, and T. Lahaye, Phys. Rev. Lett. **124**, 023201 (2020).
[33] F. M. Gambetta, W. Li, F. Schmidt-Kaler, and I. Lesanovsky, Phys. Rev. Lett. **124**, 043402 (2020).
[34] G. Birkl, S. Kassner, and H. Walther, Nature (London) **357**, 310 (1992).
[35] M. G. Raizen, J. M. Gilligan, J. C. Bergquist, W. M. Itano, and D. J. Wineland, Phys. Rev. A **45**, 6493 (1992).
[36] D. H. E. Dubin, Phys. Rev. Lett. **71**, 2753 (1993).
[37] J. P. Schiffer, Phys. Rev. Lett. **70**, 818 (1993).
[38] D. G. Enzer, M. M. Schauer, J. J. Gomez, M. S. Gulley, M. H. Holzscheiter, P. G. Kwiat, S. K. Lamoreaux, C. G. Peterson, V. D. Sandberg, D. Tupa, A. G. White, R. J. Hughes, and D. F. V. James, Phys. Rev. Lett. **85**, 2466 (2000).
[39] G. Morigi and S. Fishman, Phys. Rev. E **70**, 066141 (2004).
[40] S. Fishman, G. De Chiara, T. Calarco, and G. Morigi, Phys. Rev. B **77**, 064111 (2008).
[41] J. Sous and M. Pretko, arXiv:1904.08424.
[42] P. P. Mazza, R. Schmidt, and I. Lesanovsky, Phys. Rev. Lett. **125**, 033602 (2020).
[43] R. Belyansky, J. T. Young, P. Bienias, Z. Eldredge, A. M. Kaufman, P. Zoller, and A. V. Gorshkov, Phys. Rev. Lett. **123**, 213603 (2019).
[44] R. Moessner and S. L. Sondhi, Phys. Rev. Lett. **86**, 1881 (2001).
[45] A. Kitaev, Ann. Phys. (Amsterdam) **321**, 2 (2006).
[46] K. P. Schmidt, J. Dorier, and A. M. Läuchli, Phys. Rev. Lett. **101**, 150405 (2008).
[47] J. K. Pachos and M. B. Plenio, Phys. Rev. Lett. **93**, 056402 (2004).
[48] B. Capogrosso-Sansone, S. Wessel, H. P. Büchler, P. Zoller, and G. Pupillo, Phys. Rev. B **79**, 020503(R) (2009).
[49] H. P. Büchler, A. Micheli, and P. Zoller, Nat. Phys. **3**, 726 (2007).
[50] L. Bonnes, H. Büchler, and S. Wessel, New J. Phys. **12**, 053027 (2010).
[51] S. Will, T. Best, U. Schneider, L. Hackermüller, D.-S. Lühmann, and I. Bloch, Nature (London) **465**, 197 (2010).
[52] D. F. V. James, Appl. Phys. B **66**, 181 (1998).
[53] D. Kielpinski, B. E. King, C. J. Myatt, C. A. Sackett, Q. A. Turchette, W. M. Itano, C. Monroe, D. J. Wineland, and W. H. Zurek, Phys. Rev. A **61**, 032310 (2000).
[54] See Supplemental Material, which includes Ref. [55], at http://link.aps.org/supplemental/10.1103/PhysRevLett.125.133602 for additional details on the dynamics of a chain of trapped ions, the polaron transformation employed in Eq. (2), and the microwave dressing scheme.
[55] J. Sólyom, *Fundamentals of the Physics of Solids* (Springer, New York, 2007), Vol. 1.
[56] C. Ates, T. Pohl, T. Pattard, and J. M. Rost, Phys. Rev. Lett. **98**, 023002 (2007).
[57] I. Lesanovsky and J. P. Garrahan, Phys. Rev. A **90**, 011603 (R) (2014).
[58] M. M. Valado, C. Simonelli, M. D. Hoogerland, I. Lesanovsky, J. P. Garrahan, E. Arimondo, D. Ciampini, and O. Morsch, Phys. Rev. A **93**, 040701(R) (2016).
[59] M. Marcuzzi, J. Minář, D. Barredo, S. de Léséleuc, H. Labuhn, T. Lahaye, A. Browaeys, E. Levi, and I. Lesanovsky, Phys. Rev. Lett. **118**, 063606 (2017).
[60] M. Ostmann, M. Marcuzzi, J. P. Garrahan, and I. Lesanovsky, Phys. Rev. A **99**, 060101(R) (2019).
[61] Z.-X. Gong, G.-D. Lin, and L.-M. Duan, Phys. Rev. Lett. **105**, 265703 (2010).
[62] J. Zhang, G. Pagano, P. W. Hess, A. Kyprianidis, P. Becker, H. Kaplan, A. V. Gorshkov, Z. X. Gong, and C. Monroe, Nature (London) **551**, 601 (2017).
[63] The divergence of the shift for $\alpha \to (\alpha^*)^-$ is an artifact caused by the divergence of the characteristic length associated with the soft mode, ℓ_{soft}, which leads to the breakdown of the small displacement approximation [see Eq. (S14) of the Supplemental Material [54]]. For $r_{1,y} \approx 0.1\ \mu$m, one finds $\ell_{\mathrm{soft}}/d_{\mathrm{NN}} \approx 0.01$, which is inside the validity region of the expansion.
[64] L. L. Yan, W. Wan, L. Chen, F. Zhou, S. J. Gong, X. Tong, and M. Feng, Sci. Rep. **6**, 21547 (2016).
[65] G. Morigi and S. Fishman, Phys. Rev. Lett. **93**, 170602 (2004).